Available online at www.sciencedirect.com
SCIENCE DIRECT
Bioorganic & Medicinal Chemistry
Bioorganic & Medicinal Chemistry 14 (2006) 1792–1804

Identification of a buried pocket for potent and selective inhibition of Chk1: Prediction and verification

Nicolas Foloppe,* Lisa M. Fisher, Geraint Francis, Rob Howes, Peter Kierstan and Andrew Potter

Vernalis (R&D) Ltd, Granta Park, Abington, Cambridge CB1 6GB, UK

Received 7 June 2005; revised 10 October 2005; accepted 18 October 2005
Available online 9 November 2005

Abstract—Inhibition of the Chk1 kinase by small molecules binding to its active site is a strategy of great therapeutic interest for oncology. We report how computational modelling predicted the binding mode of ligands of special interest to the Chk1 ATP site, for representatives of an indazole series and debromohymenialdisine. These binding modes were subsequently confirmed by X-ray crystallography. The binding mode of a potent indazole derivative involves non-conventional C–H···O and N–H···π-aromatic interactions with the protein. These interactions are formed in a buried pocket at the periphery of the ATP-binding site, the importance of which has previously been overlooked for ligand design against Chk1. It is demonstrated that filling this pocket can confer ligands with dramatically enhanced affinity for Chk1. Structural arguments in conjunction with assay data explain why targeting this pocket is also advantageous for selective binding to Chk1. Structural overlays of known inhibitors complexed with Chk1 show that only the indazole series utilizes the pocket of interest. Therefore, the analysis presented here should prove helpful in guiding future structure-based ligand design efforts against Chk1.

1. Introduction

The human Chk1 kinase, which plays an essential role in the regulation of the cell cycle G2/M checkpoint,[1–10] is a promising target for the development of small molecule inhibitors against cancer.[11–20] Selective Chk1 inhibitors should also prove useful to study the regulation of the G2/M checkpoint from a fundamental biology point of view.

Only a few chemical classes acting as Chk1 inhibitors have been reported.[9,11,15–17,19,21–26] Many of these inhibitors are natural products such as debromohymenialdisine (DBH),[9] or staurosporine and its derivatives.[15–17,21–23] Crystal structures of staurosporine and two analogs bound to the Chk1 kinase domain have been described.[18] This structural information is, however, missing for the previously presented drug-like chemical series elaborated around an indazole core, which includes at least 13 compounds.[11,24] Structural information for DBH bound to Chk1 is also lacking. Importantly, the indazole series includes compound **1** (Table 1), one of the most potent Chk1 inhibitors reported to date.

We present how molecular modelling successfully predicted the binding mode of key representatives of the indazole series (compounds **1** and **2**) and DBH to the Chk1 ATP-binding site. Analysis of these docking modes in conjunction with the associated binding affinities led us to formulate a specific working hypothesis regarding ligand design against Chk1, towards improved binding affinity and selectivity. Specifically, the comparative modelling of compounds **1** and **2** pinpointed a buried pocket at the periphery of the Chk1 ATP site, suggesting convincingly that it is binding to this pocket which explains the dramatic affinity difference between these two compounds. A structural analysis of several kinase active sites, combined with assay data, also indicated that targeting this pocket ought to be advantageous for selective binding to Chk1. Therefore, the modelling work led us to devise a structure-based strategy of general interest for elaboration of Chk1 inhibitors. This strategy was vindicated when the modelled binding modes were subsequently confirmed with

Abbreviations: DBH, debromohymenialdisine; PDB, Protein data bank; RMSD, root mean square deviation; SAR, structure–activity relationship.

Keywords: Drug design; Hydrogen bonds; Molecular modelling; Molecular recognition; Oncology; X-ray crystallography.
* Corresponding author. Tel.: +44 1223 895 338; fax: +44 1223 895 556; e-mail: n.foloppe@vernalis.com

0968-0896/$ - see front matter © 2005 Elsevier Ltd. All rights reserved.
doi:10.1016/j.bmc.2005.10.022

Table 1. Structures of compounds **1–3** and their binding affinities[a] to kinases of interest

Compound	Structure	K_i (μM)	IC_{50} (μM)						
		Chk1	Chk1	CDK1	CDK2	$GSK3_\beta$	PDK1	Akt1	PKA
1	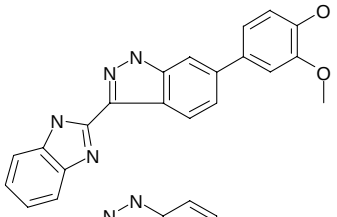	0.026 (0.005)	0.042 (0.013)	0.040 (0.018)	0.104 (0.039)	0.314 (0.066)	0.443 (0.142)	23.600 (1.840)	171.719 (38.850)
2	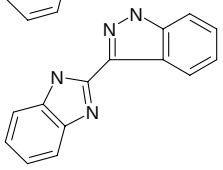	8.580 (3.060)	6.296 (4.160)	0.845 (0.200)	14.309 (5.529)	0.744 (0.166)	2.706 (2.100)	>50	>200
3 (DBH)	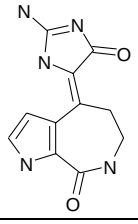	0.659 (0.021)	0.353 (0.285)	0.266 (0.096)	0.856 (0.788)	0.168 (0.013)	8.830 (0.495)	>50	0.190 (0.760)

[a] Every reported affinity is the average of at least two measurements, with standard deviations given in parentheses.

X-ray crystallography. As predicted, the X-ray binding mode includes a number of non-conventional protein–ligand interactions such as C–H···O and N–H···π-aromatic interactions. The present work also provides new and careful determinations of the affinities of compounds **1**–**3** for Chk1.

Structural overlays of the known chemical inhibitors complexed to Chk1 show that only the indazole series takes advantage of the pocket of interest. This suggests that there is scope for further elaboration of other inhibitors, and will provide helpful guidance for future structure-based design efforts towards more potent and selective Chk1 inhibitors.

2. Results and discussion

Given the excellent agreement between predicted modelled binding modes and their subsequently determined X-ray counterparts (see Section 2.2), only the X-ray binding modes are shown (Figs. 1, 2 and 4).

Compounds **1** and **2** were prepared by previously published literature routes[24,27] (see Methods and Schemes 1–3).

2.1. Binding affinities of selected indazole compounds and DBH

Compounds **1** and **2** inhibit human Chk1 in an ATP-competitive manner, with K_i values of 0.026 and 8.58 μM, respectively (Table 1). Each K_i was derived from several independent measurements confirming that compound **1** is a potent Chk1 inhibitor, although its affinity appears to be six times less than previously reported.[11,24] The affinity for Chk1 of the core of the indazole series (**2**), presented here for the first time, is important to interpret the SAR of substituents grafted on this core. Indeed, the influence of the substituents on affinity can only be deduced if the affinity of the core itself is known. This shows that the additional methoxyphenol moiety in compound **1** leads to a 330-fold increase in affinity for Chk1. It is therefore important to characterize the structural positioning of this methoxyphenol in its Chk1-binding site, to gain a better understanding of the factors which lead to such a dramatic increase in affinity.

DBH was also found to inhibit Chk1 in an ATP-competitive manner, confirming a previous report which characterized the binding of DBH to Chk1 in terms of an IC_{50}.[9] We obtained a K_i of ~0.6 μM for the affinity of DBH to Chk1.

2.2. Prediction and confirmation of the binding mode of the indazole scaffold

Compounds **1** and **2** were initially docked computationally into the ATP-binding site of the crystal structure of apo human Chk1 (PDB[28] entry 1IA8[29]). This suggested convincing binding modes for compounds **1** and **2**, in view of their sensible interactions with the protein, which could explain the affinity difference between **1** and **2** (Section 2.4). The root mean square deviation (RMSD) between the predicted and X-ray coordinates of compounds **1** and **2** was ~0.4 Å (see Methods and Supplementary Information). Although the X-ray structure of the Chk1-compound **1** complex is of medium resolution (Table 2), the crystallographic electron density maps clearly support the conformation of the methoxyphenol of compound **1** as shown in Figure 2, as well as the orientation of the protein backbone for residues Ser147 and Asp148. These peptide units adopt the same conformation in Chk1 X-ray structures of better resolutions.[18,25,29]

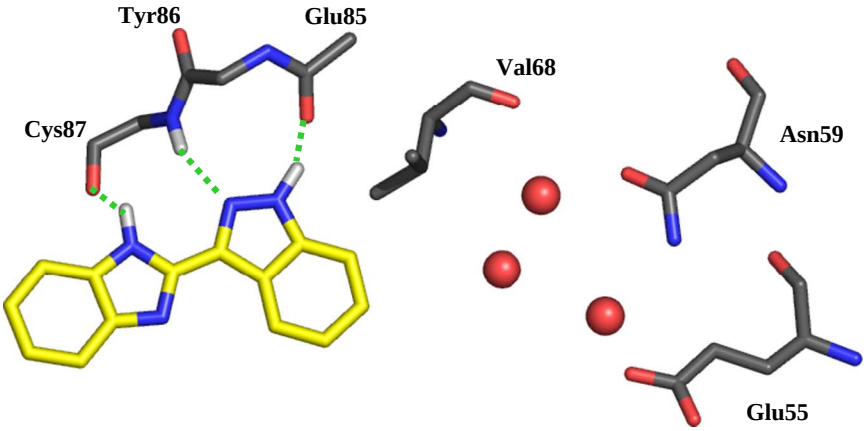

Figure 1. Crystallographic binding mode of compound **2** in the ATP-binding site of Chk1. For clarity, only selected residues and hydrogen atoms are shown. Hydrogen bonds between the compound and the kinase backbone are depicted with green dotted lines. The three red spheres represent water molecules. The shown protein residues are labeled.

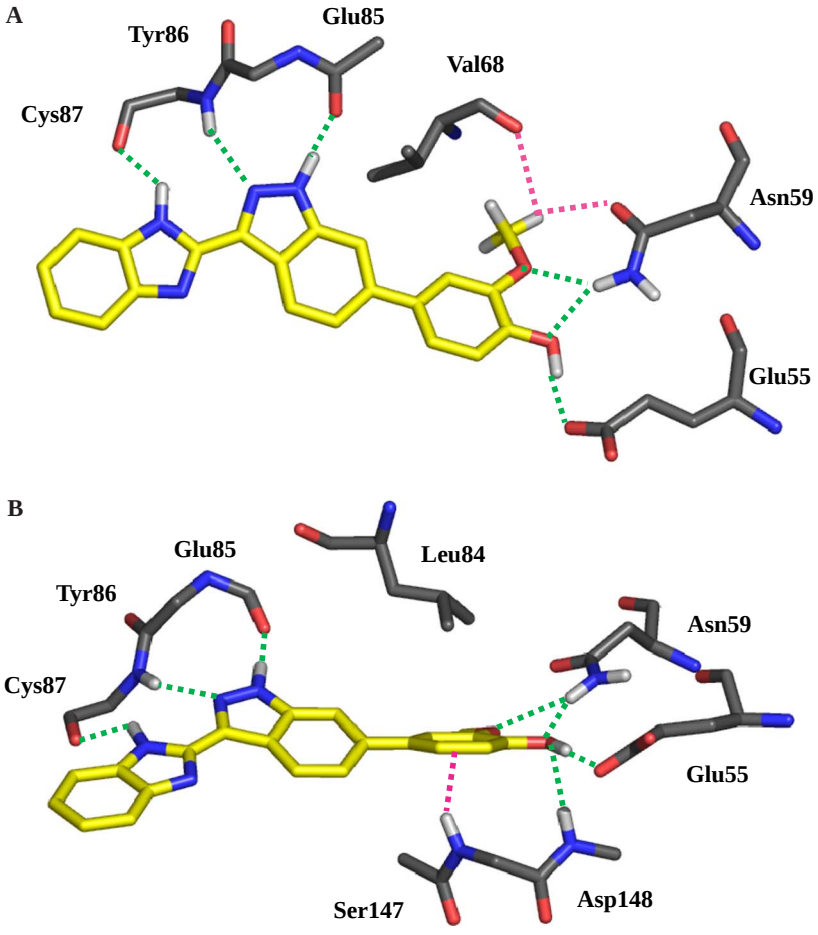

Figure 2. (A and B) Different views of the crystallographic binding mode of compound **1** in the ATP-binding site of Chk1. For clarity, only selected residues and hydrogen atoms are shown. Conventional hydrogen bonds between the compound and the protein are depicted with green dotted lines, while C–H···O and N–H···π-aromatic electron interactions are traced in magenta. For the N–H···π-aromatic interaction, the phenyl ring is represented by its centroid. The shown protein residues are labelled.

The indazole core of **1** and **2** largely overlaps with the volume typically occupied by the adenine base of ATP when complexed to kinases, with the indazole hydrogen-bonded to the highly conserved kinase backbone motif at the hinge between the two lobes of the kinase domain (Fig. 1). The hydrogen-bond interactions between inda-

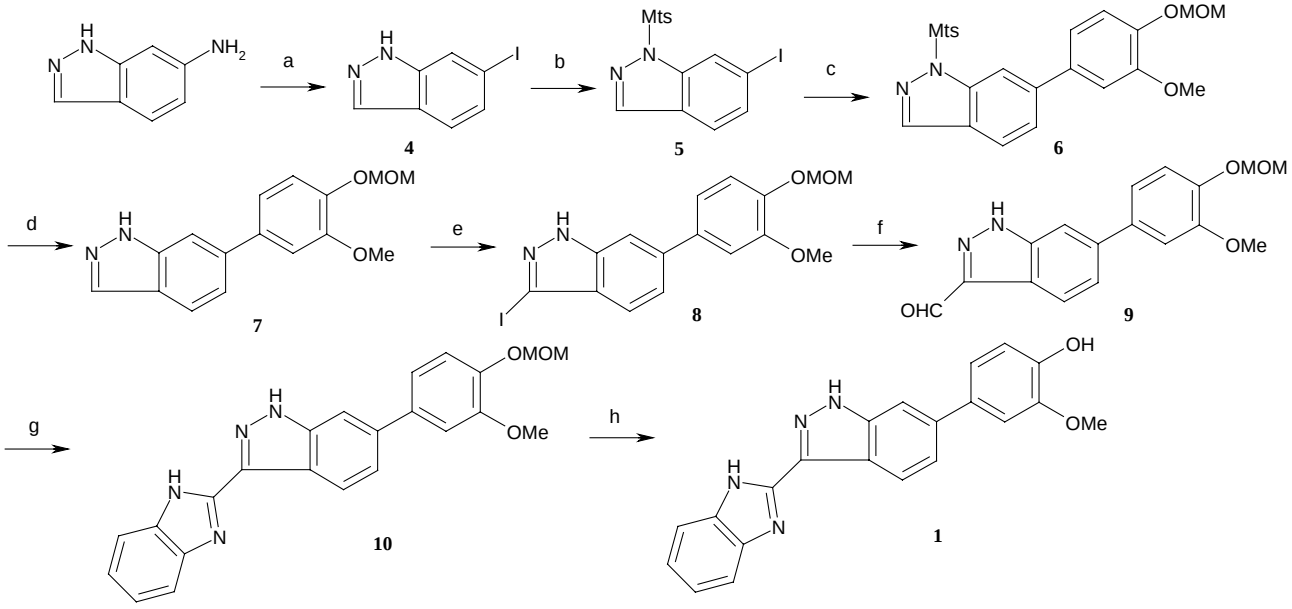

Scheme 1. Reagents and conditions: (a) Concd HCl (aq), $NaNO_2$, KI, H_2O, 0–50 °C, 3 h, (39%); (b) NaO*t*Bu, MtsCl, THF, 0–23 °C, 2.5 h, (92%); (c) (**12**), $PdCl_2(PPh_3)_2$, Et_3N, K_2CO_3, dioxane/H_2O, 90 °C, 2 h; (d) NaOH, MeOH, 45 °C, 1 h, (27%); (e) I_2, NaOH, dioxane, rt, (42%); (f) PhLi, *s*-BuLi, DMF, THF, −78 °C to rt, 18 h; (g) 1,2-diaminobenzene, $CuAc_2$, AcOH, MeOH/H_2O, rt, 19 h (21%); (h) TFA/THF, H_2O (28%).

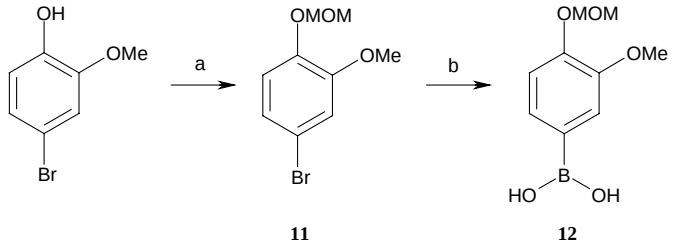

Scheme 2. Reagents and conditions: (a) methoxymethyl chloride, KOH(s), H_2O, Bu_4NBr, DCM, 0 °C to rt, 64 h, (93%); (b) *n*-BuLi, $B(OMe)_3$, THF, −78 °C to rt, 20 h, (68%).

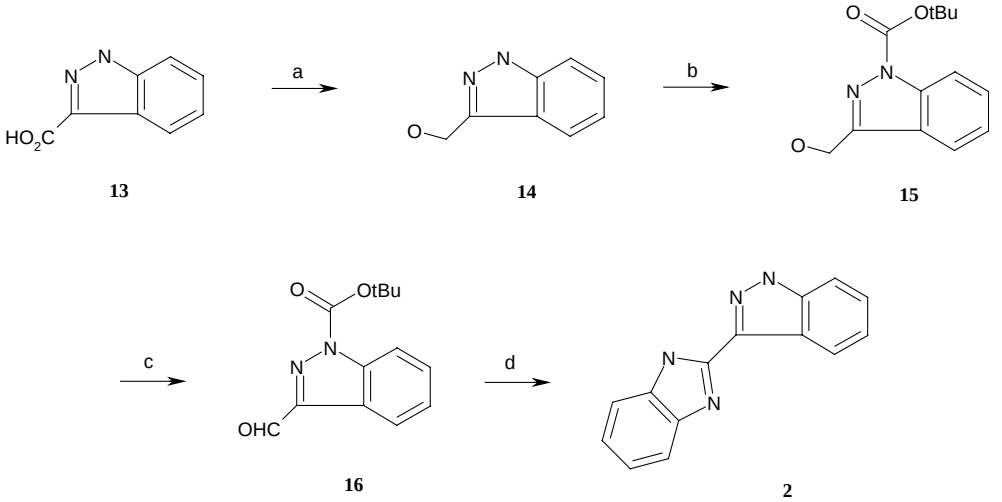

Scheme 3. Reagents and conditions: (a) $LiAlH_4$, 0 °C, THF, 50%; (b) $(BOC)_2O$, THF, 60%; (c) IBX, THF, △, 70%; (d) *o*-phenylenediamine, sulfur, DMF, 95 °C, 55%.

Table 2. Crystallographic data collection and refinement statistics for Chk1 in complex with compounds **1**–**3**

Structure	Chk1 + compound		
	1	**2**	**3** (DBH)
Data collection statistics			
Resolution (Å)	2.60	2.35	2.05
Measured reflections	117777	57350	117609
Unique reflections	9736	14217	19586
Completeness: overall/in hrb* (%)	96.7/87.1	95.1/82.9	98.1/99.8
Average multiplicity/in hrb	4/2	2/1	4/4
Mean $I/\sigma I$: Overall/in hrb	12.7/2.6	9.6/3.7	14.7/2.4
R_{merge}: Overall/in hrb (%)	8.8/38.8	8.9/35.2	7.8/45.1
Refinement statistics			
R_{free} (%)	29.0	27.5	26.2
R_{cryst} (%)	22.2	19.3	18.2
Rms deviations:			
Bonds (Å)	0.025	0.018	0.022
Angles (°)	2.289	1.645	2.100
B Factor (Å^2)	3.137	2.424	3.095
PDB Code	2C3L	2C3K	2C3J

R_{free} is the *R* factor calculated using 5% of the reflection data chosen randomly and omitted from the refinement process, whereas R_{cryst} is calculated with the remaining data used in the refinement. Rms bond lengths and angles are the deviations from ideal values; the rms deviation in *B* factors is calculated between covalently bonded atoms.

* hrb, highest resolution bin.

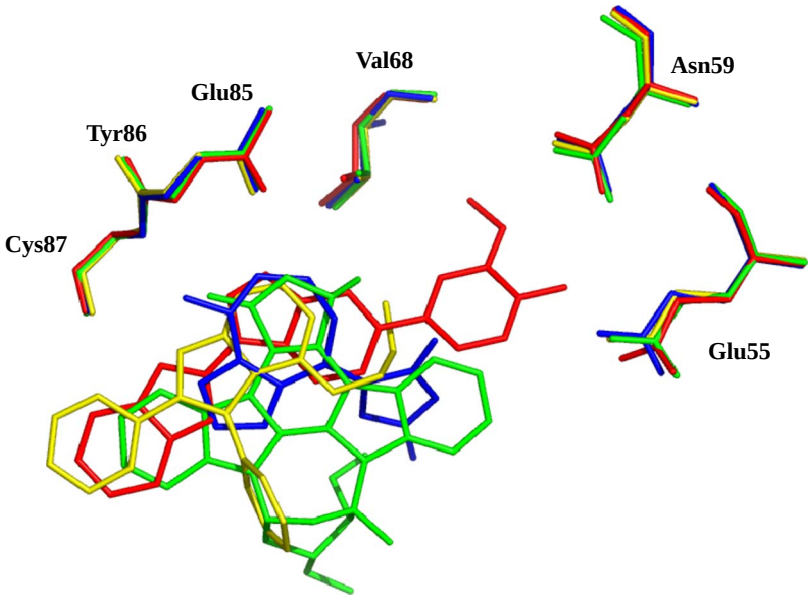

Figure 3. Superposition of the crystal structures of Chk1 in complex with compound **1** (red), DBH (blue), staurosporine (green; PDB entry 1NVR[18]) and compound **17** (yellow; PDB entry 2BRB[25]). Compound **17** is shown in Scheme 4. Only selected protein residues are shown and labelled.

zole and protein define the tautomer of the bound form of the indazole. In the X-ray structure of compound **2**, three water molecules were located in the buried pocket lined by Glu55, Asn59 and Val68. These water molecules are displaced by the methoxyphenol of compound **1** when bound to Chk1 (Fig. 2). This pocket filled by the methoxyphenol of **1** is not occupied by other Chk1 ligands for which X-ray binding modes are available (Fig. 3). Therefore, the elucidation of the binding mode of compound **1** provides new structural insights relevant to ligand design against Chk1. Transferring elements of the binding mode of compound **1** to other chemical series of Chk1 inhibitors, by filling the buried pocket, could confer increased affinity for Chk1 to these series.

A recently reported inhibitor (**18**, Scheme 4), with an affinity of 0.450 μM for Chk1,[19] contains a methoxyphenyl analogous to the methoxyphenol of **1**. This prompted us to test whether **18** could be docked in the Chk1 ATP site, with its methoxyphenyl group in a position similar to that of its counterpart in **1**. Two sensible docking modes of **18** to Chk1 were obtained (see Supporting Information), with the central pyrimidine hydrogen-bonding the conserved kinase backbone motif as expected, and reasonable interactions between the phenyl rings and the protein. The geometric constraints associated with these docking modes, however, do not allow the methoxyphenyl group to access the pocket discussed in this work. Therefore, we predict that the chem-

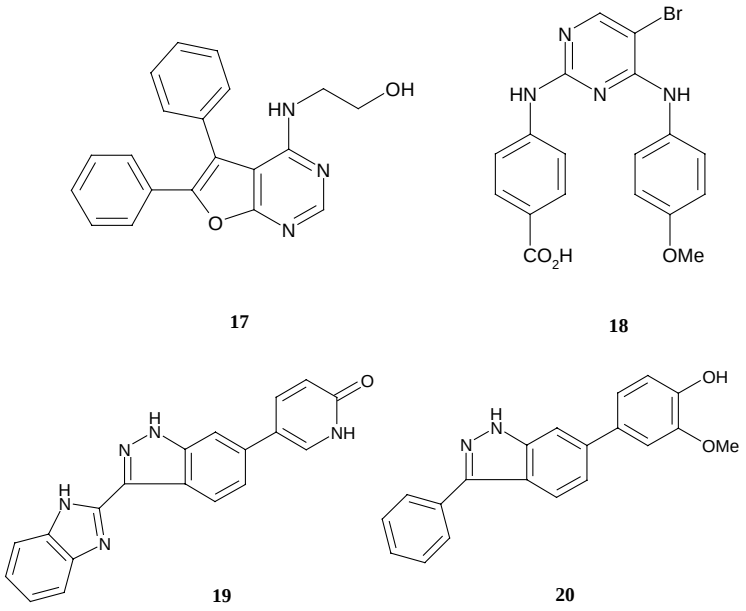

Scheme 4.

ical series represented by **18** is another chemotype which does not utilize this pocket.

2.3. Prediction and confirmation of the binding mode of DBH

The overall binding mode of DBH was also predicted by docking to the ATP binding site of the crystal structure of apo human Chk1 and confirmed by X-ray crystallography (Fig. 4). Although essentially correct, this prediction was less accurate (RMSD ~1.2 Å) than with the indazole compounds, partly because of flexibility in the seven-membered ring and the water-mediated hydrogen bond between DBH and the protein backbone in the X-ray structure. Given the pseudo-symmetry of its hydrogen-bond donating and accepting groups, the fused ring system of DBH could also dock to the kinase backbone in another orientation, by flipping around the N^{Cys87}–H···O hydrogen bond. The hydrogen bonds between the imidazolone ring of DBH and Lys38, Asn135

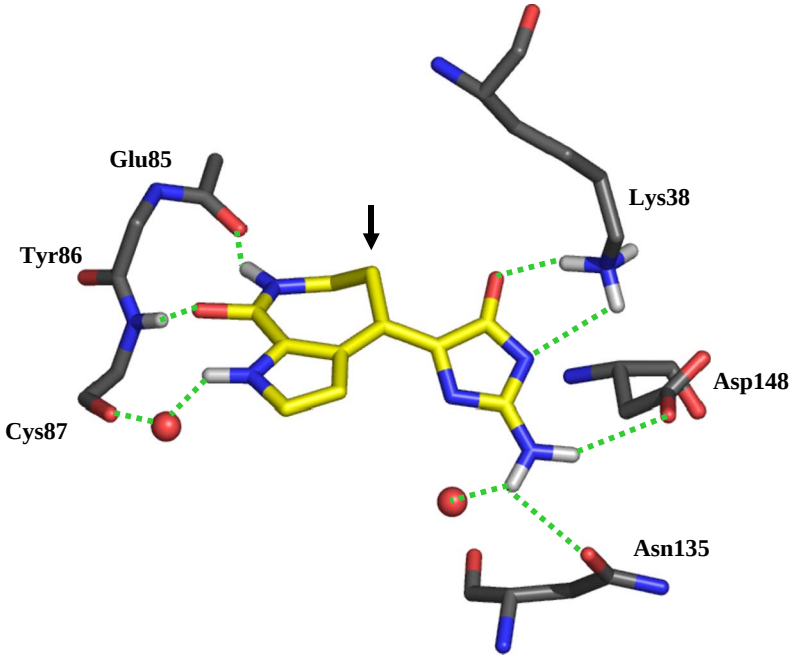

Figure 4. X-ray binding mode of debromohymenialdisine (DBH) to Chk1. For clarity, only selected residues and hydrogen atoms are shown. Hydrogen bonds between the DBH and the protein or water molecules are depicted with green dotted lines. The red spheres represent water molecules. Selected protein residues are labelled. The black arrow points to the carbon which could be derivatised towards the buried pocket discussed in this work.

and Asp148 select between the two possible orientations of the fused ring system (Fig. 4).

The relatively high number of hydrogen bonds between DBH and Chk1 is associated with a rather modest binding affinity (Table 1). This is compatible with some evidence indicating that protein–ligand hydrogen-bonding may favour protein–ligand association only weakly.[25,30–32] DBH does not fill the pocket occupied by the methoxyphenol of compound **1**. This suggests that opportunities may exist to enhance DBH affinity against Chk1 by reaching into the pocket of interest. From a purely structural point of view it may be possible to derivatise from the seven-membered ring which offers at least one C–H vector pointing towards the pocket (Figs. 3 and 4). In that context the exact conformation of the fused ring of DBH, when bound to Chk1, is important. The crystallographic electron density does support the puckering of the seven-membered ring shown in Figure 4.

2.4. Non-conventional C–H···O and N–H···π interactions

The details of the interactions of the methoxyphenol with the Chk1-binding pocket (Fig. 2) are of great interest because they are associated with a dramatic increase in affinity for Chk1, as well as an influence on the binding selectivity across different kinases (Table 1 and Section 2.6). The methoxyphenol fits very snugly in its binding pocket, with its polar groups forming extensive hydrogen bond interactions with Glu55, Asn59, and Asp148. All the hydrogen-bonding capabilities of the ligand hydroxyl are fulfilled by donating to the carboxylate of Glu55 and accepting from the side-chain amide of Asn59 and the backbone amide of Asp148. Asn59 side chain donates a proton to both the hydroxyl and methoxy oxygens in a bifurcated hydrogen bond. The methyl group of compound **1** has non-polar contacts with the side chains of Val68 and Leu84. This methyl group, polarised by the oxygen atom to which it is attached, may form favourable weak polar C–H···O interactions, with some hydrogen-bonding character, with the carbonyl oxygens of Val68 and the side chain of Asn59. Although this type of interaction has been well documented in the arena of small organic molecules for some time,[33–37] the recognition of its interest in protein–ligand recognition for drug design is more recent [38–40] and controversial. It is striking that the methyl group of **1** contacts two carbonyl oxygens, which are otherwise hydrated (Fig. 1).

Arguably even more unusual is the phenyl ring of the methoxyphenol being sandwiched between the apolar side chain of Leu84 and the polar amide N–H of Ser147, with this N–H pointing toward the phenyl π-aromatic electrons. The distance between the nitrogen and the ring centroid is 3.5 Å, with an N–H···centroid angle of 141.5°. This provides an unambiguous example where a ligand phenyl ring acts as a hydrogen bond acceptor. Although this type of interaction has already been recognised,[41–44] very few examples have been reported mediating protein–ligand complexes. The interaction between Leu84 and the methoxyphenol might also involve C–H/π interactions, which are known to be more favourable than the associated van der Waals dispersion contribution.[45–47]

The excellent structural complementarity between the methoxyphenol moiety and its binding pocket, where all elements of the protein form potentially favourable interactions with the ligand, is consistent with the associated large difference in Chk1 affinity between **1** and **2**. Other factors contributing to this affinity gain probably include desolvation of the ligand phenyl and methyl groups, and possibly an entropy gain upon displacement of the water molecules[48] which otherwise fill this pocket (Fig. 1). Using relatively apolar ligand functionalities to interact with buried protein polar groups is likely to be favourable from a ligand desolvation point of view, and may be a strategy of general interest to target this pocket.

A notable consequence of the interactions described above is that an aromatic, rather than an aliphatic, ring may be required to fill the pocket lined by the side chain of Leu84 and the backbone of Ser147. Indeed, only the π electrons of an aromatic moiety would accommodate a hydrophobic contact on one side while being faced by a hydrogen bond donor on the other side. Also, basic stereochemistry suggests that an aliphatic ring may be too thick to fit sterically in the pocket. Pyrazole rings and analogues with both an accepting and a donating nitrogen may be well suited to hydrogen-bond the side chain of Asn59.

2.5. Consistency between SAR and binding mode for the indazole series

Elements of SAR around the indazole series represented by compound **1** were summarized previously (Table 5 in Li and Zhu[11]). The majority of the analogues of **1** had affinities for Chk1 in the low nanomolar range. In all these potent analogues, the phenol ring is derivatized with relatively small hydrophobic substituents which fit sterically (not shown) in the pocket discussed in this work, consistent with the associated high affinities and the binding mode in Figure 2. The small affinity differences between these compounds are, however, too subtle to be explained only based on simple stereochemical criteria.

Compound **19** (Scheme 4) is an intriguing exception, because it has a much lower reported affinity for Chk1 (1.1 μM), despite enough room in the protein pocket to accommodate its pyridone ring. The most stable form of **19** bound to Chk1 is unclear, due to the tautomeric equilibrium between pyridone and pyridol. Although 2-pyridone is intrinsically marginally more stable than 2-hydroxypyridine in gas phase,[49] the pyridone-pyridol equilibrium is strongly affected by the environment and substituents.[50] Modelling of the bound pyridone tautomer shows that its amide nitrogen would be buried without hydrogen-bonding partner, suggesting that desolvation of the pyridone would strongly weaken its binding to Chk1. Compound **19** would fit better in the pocket as a pyridol because the pyridol nitrogen could hydrogen-bond to Lys38 (not shown). However, this is

still compatible with the weak affinity of **19** if it exists primarily as a pyridone in aqueous solution.

The other notable loss of affinity was observed for the analogue of **1** where the benzimidazole was replaced by a phenyl[11] (compound **20**, Scheme 4), which can be explained by the binding mode of **1**, for instance because of the lack of hydrogen bond between a phenyl and the kinase backbone.

To recapitulate, the compounds reported in Table 5 from Li and Zhu[11] can be grouped in two sets: (i) those with high affinity ($K_i < 0.1$ μM) which are all derivatised with small hydrophobic substituents which fit in the pocket of interest and (ii) compounds **19** and **20** (Scheme 4) which have much lower affinities, consistent with the binding mode of **1** and the above arguments. Therefore, the major trends in the SAR around compound **1** are consistent with the binding mode of this compound. Detailed calculations, such as free energy perturbation,[51,52] may be able to provide additional insights into the subtle affinity differences between the most potent compounds in this series, but this is beyond the scope of this work. Also, one would need to consider possible uncertainties in the experimental affinities, given that the present work finds that the affinity of **1** is six times less than previously reported.[11,24]

2.6. Influence of the pocket on the selectivity of binding

Different kinases are involved in a variety of cell signalling pathways[53] but X-ray structures combined with sequence alignments have shown that many features of the ATP-binding pocket tend to be conserved across kinases.[54–56] Therefore, selectivity of inhibition for a particular kinase is a well-known issue, and we investigated this question for Chk1 by comparing the IC_{50}'s of compounds **1**–**3** for several kinases (Table 1). One of the criteria to select the kinases for which selectivity data were obtained was that an X-ray structure should be available for their ATP-binding site, with the exception of cyclin dependent kinase 1 (CDK1, also called Cdc2). This should allow insights regarding the influence on selectivity of the Chk1 pocket filled by the methoxyphenol of **1**, by comparison to its counterpart in other kinase structures. The specific role of this pocket for selectivity may be dissected, to some degree, by comparing the IC_{50}'s of compounds **1** and **2**. This can only be a qualitative analysis because there is more to selectivity than simple steric interactions between a ligand and the residues that it contacts directly. For instance overall protein dynamics, with elements of induced fit, may contribute to selectivity. It remains that, given the dramatic potency enhancement achieved by filling the pocket of interest in Chk1, it is of direct practical interest to estimate the potential of this pocket for selectivity gains when targeting Chk1.

In particular, the rationale for Chk1 inhibition in the context of oncology is to abrogate the ability of tumour cells to arrest in G2 in response to DNA damage.[11,12,57] This is incompatible with a concomitant inhibition of Chk1 and CDK1, because active CDK1 is necessary for the G2 to M transition.[58–60] Therefore, selectivity data versus CDK1 are of particular interest. Unfortunately, a crystal structure of CDK1 is, to our knowledge, not available. Therefore, an homology model of human CDK1 was built based on a crystal structure of human cyclin dependent kinase 2 (CDK2) bound to cyclin A. This utilizes the 66.2% sequence identity between CDK1 and CDK2. There is no notable sequence difference between CDK1 and CDK2 for the residues lining the pocket of interest, and the homology model of CDK1 is very similar to its CDK2 template in this region. The selectivity data are discussed assuming that compounds **1**–**3** adopt similar binding modes with different kinases.

The lack of affinity of **1** and **2** for Akt (protein kinase B) and PKA can be understood in view of the steric clash between the benzimidazole of **1** and **2** and Phe439 (Akt) or Phe327 (PKA) (Fig. 5). With other kinases compound **2** tends to exhibit affinities closer to that for Chk1, although showing elements of selectivity. In particular, compound **2** is 7-fold more potent for CDK1 than Chk1. This difference is lost with the more potent compound **1** (Table 1), which implies that larger potency gains are made for Chk1 than for CDK1 by binding of the methoxyphenol to its pocket. The notion that the interactions of the methoxyphenol with its pocket are less favourable in CDK1 than in Chk1 is consistent with the replacement of Leu84/Asn59 in Chk1 by Phe80/Leu55 in CDK1 (Fig. 5). The replacement of Asn59 by an apolar side chain leads to a loss of two conventional hydrogen bonds between the protein and compound **1**. In addition, the replacement of Leu84 (Chk1) by the bulkier Phe80 (CDK1) may lead to steric hindrance between compound **1** and CDK1, as suggested by a comparison of the similar Chk1/CDK2 pair. This is not sufficient, however, to obtain the desired selectivity between Chk1 and CDK1 with **1**, given that it exhibits the same IC_{50} for both proteins. This result puts the indazole series of Chk1 inhibitors in a new light, suggesting deficiencies in its therapeutic selectivity profile. In addition, this chemical series can only be a blunt instrument if used as a pharmacological tool to study the mechanisms and regulation of the G2/M checkpoint. The present work also highlights that obtaining an X-ray structure for CDK1 would help in the design of therapeutically relevant Chk1 inhibitors.

That the Chk1 pocket lined by Asn59 and Leu84 plays a role regarding selectivity is confirmed by the IC_{50}'s of **1** and **2** with CDK2, $GSK3_\beta$ and PDK1. These proteins have an apolar side chain in place of Asn59 (Chk1), consistent with much lower affinities of **1** for these proteins. Taken together, these results strongly suggest that the pocket discussed in this work is of great practical importance to design ligands with a high degree of selectivity for Chk1. This may help to convert DBH and other compounds into a Chk1 selective inhibitor.

3. Conclusions

This work reports the crystal structures of DBH and key representatives of an indazole series of Chk1 inhibitors

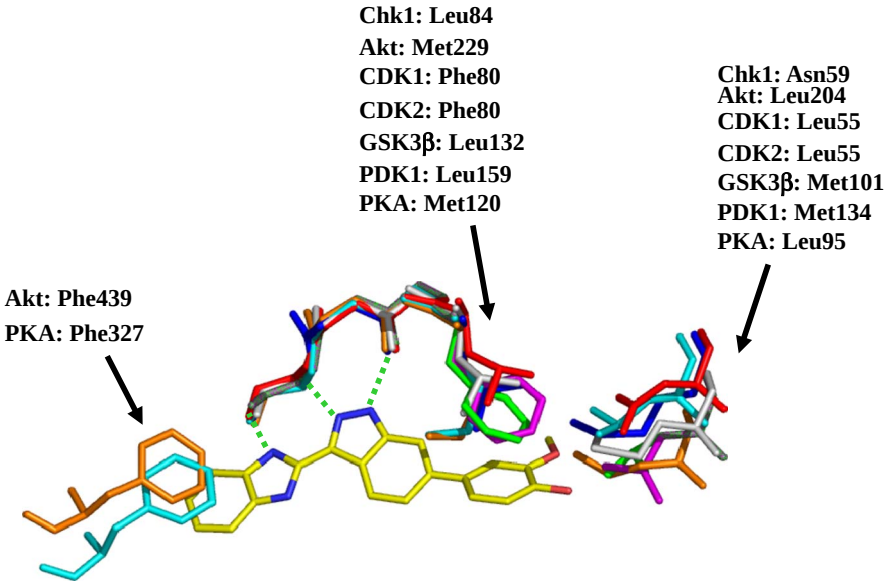

Figure 5. Superposition of Chk1 structure (red) with those of kinases Akt (cyan), CDK1 (magenta), CDK2 (green), GSK3β (light grey), PDK1 (dark blue) and PKA (orange). X-ray structures of Chk1, Akt, CDK2, GSK3β, PDK1 and PKA are from PDB entries 1IA8,[29] 1O6L,[82] 1OI9,[67] 1Q5K,[83] 1H1W[84] and 1ATP,[85] respectively. For CDK1, a homology model based on CDK2 is used. The conserved hinge backbone, to which compound **1** is hydrogen bonded (green dotted lines) in Chk1, is closely aligned across all proteins. Only selected protein side chains in the vicinity of compound **1** are shown and labelled. These side chains are those structurally aligned with Asn59 and Leu84 of Chk1, which are in direct contact with the methoxyphenol of compound **1**. Phe439 (Akt) and Phe327 (PKA) are also shown because they have no structural equivalent in the other kinases considered here.

complexed with this human kinase ATP-binding site. The binding modes of these ligands, and their implications for ligand design, had been predicted accurately by computer modelling well before the crystal structures were obtained, providing an example of a helpful bona fide prediction verified by experiment. This was supplemented by careful measurements of the associated binding affinities, and the actual affinity of **1** for Chk1 is six times less than previously reported.[11,24] Compound **1**, however, remains one of the highest affinity ligands for Chk1, and comparing the binding modes and affinities of **1** and **2** led to new and helpful insights.

The binding mode of **1** revealed a buried pocket which can be used to gain dramatic affinity increases against Chk1. Interestingly, it is compatible with a number of non-conventional interactions between **1** and the protein pocket. In particular, this provides a rare non-ambiguous example of an N–H···π-aromatic interaction with hydrogen bond character between ligand and protein, which is probably important to retain high binding affinity while filling this pocket. In addition, C–H···O interactions were observed, which may also present a weak hydrogen bond character.

The comparison of the residues lining the Chk1 pocket of interest to their counterpart in a few other kinases suggests that targeting this pocket should strongly influence the binding selectivity. This was born out by comparing the affinities of **1** and **2** for these kinases. This analysis suggests that, although the affinity of **1** is similar for Chk1 and CDK1, its interactions with the pocket moderately favour binding to Chk1. This is notable because the biological rational for targeting Chk1 against cancer probably requires ligands which discriminate between Chk1 and CDK1.

It is striking that the pocket of interest is not filled by the ligand in any of the other Chk1-ligand X-ray structures reported so far, and this covers the majority of the current chemical series of Chk1 inhibitors. This means that there may be scope for further elaborations of some of these series, including DBH which has a relatively low molecular weight. The X-ray structure of DBH bound to Chk1 provides a firm structural basis for derivatisation of DBH towards the pocket highlighted in the present work.

4. Computational and experimental methods

4.1. Molecular modelling

Docking was performed with the program rDock which is an extension of the program RiboDock,[61] using an empirical scoring function calibrated based on protein–ligand complexes.[62,63] The Monte Carlo/simulated annealing protocol initially used in RiboDock was replaced by a steady state Genetic Algorithm (GA) to improve the efficiency of the docking search. Ligand docking poses were represented using a conventional chromosome representation of translation, rotation and rotatable bond dihedral angles. A single GA population was used, of size proportional to the number of ligand rotatable bonds, with a mutation:crossover ratio of 3:2. The overall orientation and internal conformation of the compounds were searched with the GA, while the protein was kept fixed.

Docking used the ATP-binding site in the crystal structure of apo human Chk1 (PDB[28] entry 1IA8[29]). Water molecules were removed from the coordinates and polar hydrogens added to the protein using the CHARMm force-field.[64] To specify the docking volume, the ATP-bound crystal structure of protein kinase A (PDB entry 1ATP) was superimposed onto that of Chk1. There was unambiguous superimposition of the ATP-binding sites and the docking volume in Chk1 was defined as the space within 8 Å of the ATP molecule. Before docking, the three-dimensional structure of the compounds was built with the software MOE[65] and energy minimized with the Merck molecular force-field.[66] Several low energy conformations were generated for the flexible seven-membered ring of DBH and all of them were docked. Each compound was subjected to 200 docking runs, and the output docking modes were analyzed by visual inspection in conjunction with the docking scores. The best scoring docking modes were selected as working hypothesis for compounds **1**–**3**, because they were structurally sensible and compatible with the few elements of SAR available.[11] In addition, there was relatively little variation in the docking output and no alternative plausible docking mode was generated for compounds **1** and **2**. The RMSD on non-hydrogen atoms between modelled and X-ray binding modes for the ligands were calculated after best fit of the protein structures on all atoms of the backbone of the conserved kinase motif (Glu85-Tyr86-Cys87), using MOE. Hydrogen atoms shown in Figures 1,2 and 4 were added to the X-ray coordinates with the software MOE and the Merck molecular force-field. Compound **18** was docked to the same protein structure used to dock compounds **1**–**3**.

Modeling of the three-dimensional structure of human CDK1 was carried out by comparative homology modelling, using as template a crystal structure of CDK2 in complex with cyclin A (PDB entry 1OI9,[67] resolution 2.10 Å). This template was selected because the assays involving CDK1 were performed with an homologous CDK1/cyclin B complex. The sequence of human CDK1 was retrieved from the SWISS-PROT data bank[68] (Accession No. P06493), and shares 66.2% identity with that of CDK2 (shortest sequence used for total length), which provides a sound basis for comparative modelling.[69,70] This allowed an unambiguous sequence alignment for the region encompassing the binding site of interest, and 10 structural models were generated with previously described algorithms,[71,72] as implemented in MOE.[65] The default parameters of the program were kept. The 10 CDK1 models did not vary significantly in the region of interest and the best scoring model (as reported by MOE) was used for comparison with the other kinases (Fig. 5).

Pictures of three-dimensional molecular structures were prepared with PyMOL.[73]

4.2. Kinase assays for IC_{50} determinations

Enzyme inhibition assays to determine IC_{50}'s with Chk1, CDK1/Cyclin B and PKA were performed as described previously,[25] and equivalent assays with other kinases were performed in a similar manner. For the GSK3β assay, GSK3β (Upstate) was used at 4 nM with 2.5 μg phosphor-glycogen synthase peptide-2 (Upstate) at a final ATP concentration of 100 μM. The reaction was incubated for 30 min at rt. For the PDK1 assay, PDK1 (Upstate) was used at 14 nM with 5 μM PDKtide (Zinsser Analytical; sequence YRRAAVPPSPSSLSRHSSPHQ(P)SEDEEE) at a final ATP concentration of 10 μM. The reaction was incubated at 30 °C for 30 min. For the Akt1 assay, 3 nM Akt1 (Upstate) was used with Histone H1 as substrate with a final ATP concentration of 200 μM. The reaction was incubated at 30 °C for 40 min. For the CDK2/Cyclin A assay, CDK2/Cyclin A obtained in-house was used at 9.5 nM with CDKtide as a substrate at a final ATP concentration of 100 μM. The reaction was incubated at 30 °C for 40 min.

Debromohymenialdisine (DBH) from *Stylotella aurantium* was purchased from Calbiochem (Catalogue No. 252010), with a purity of 96.8% by HPLC.

4.3. Chk1 K_i determinations

Chk1 kinase assays were performed as described previously[25] in a final reaction volume of 50 μl. Chk1 was used at 18 nM and the reaction was incubated at 30 °C for 30 min. For K_i determinations a matrix of inhibitor and substrate concentrations were tested. Inhibitor concentrations were tested from four times IC_{50} with 0.6-fold dilutions over 7 concentrations, as well as a final reaction with no inhibitor present. Substrate concentrations ranged from $0.5 \times K_m$ to $8 \times K_m$.

Due to the inherent errors that occur with traditional methods of analysis of linearised versions of the Michaelis–Menten equation (Lineweaver–Burk, Eadie–Hofstee), more direct methods relying on nonlinear regression analysis applied to the whole data set simultaneously are known to be more accurate.[74] We have used such a non-linear regression analysis for K_i determinations, following a 4-step process:

(i) An estimate of the V_{max} and K_m of Chk1 was obtained in the absence of inhibitor, using the Michaelis–Menten steady state equation (model 253; XLFit 4,[75] ID Business Solutions, Guildford, UK).
(ii) For each inhibitor, an initial suggested mode of action was inferred from analysis of double reciprocal Lineweaver–Burk plots. A competitive mode of action was suggested in all cases, however, a non-competitive mechanism was not ruled out in subsequent steps.
(iii) Then the experimental data were fitted alternatively to a competitive and a non-competitive equation using a 3D non-linear regression (XLFit 4, IDBS). For the non-competitive model, Eq. 4 from Kakkar et al.[86] was used. For the competitive model we used the Michaelis–Menten substrate plus inhibitor equation (Model 12; Life Science Workshop Toolbox, MDL Information Systems Inc., USA)

$$y = V_{max}/(1 + (K_{m1}/x1) * (1 + x2/K_i)),$$

where $x1$ = [ATP]; $x2$ = [Inhibitor] and $y = CPM_{corrected}$. K_{m1} is the Michaelis constant for the enzyme–substrate

pair, and K_i is the dissociation constant for the enzyme–inhibitor pair. By definition, competitive inhibition can be surmounted by increasing the concentration of substrate. Consequently, a competitive inhibitor does not alter V_{max}. The data set was processed against both models using a free-fit initially and the K_m and V_{max} in the absence of inhibitor were obtained. In all cases, the V_{max} obtained from the non-linear regression was close to the V_{max} calculated in step i). Three-dimensional plots were produced with both the competitive and non-competitive models with x-axis = [ATP], y-axis = [I] and z-axis = $CPM_{corrected}$.
(iv) To confirm which model fitted the data best, several statistical parameters were checked: the normalized χ^2, F-Test and T-Test. In view of these statistical tests, each compound fitted preferentially to a competitive mode of action model, consistent with the X-ray structures. K_i values were then obtained from the relevant model.

4.4. Crystallisation and three-dimensional structure determination

Chk1 1-289 was expressed, purified and crystallised as previously described.[25]

Protein–ligand complex data sets were collected at cryo-temperature. Reservoir solution with 20% glycerol added was used as the cryoprotectant. Data were collected either on our in-house detector (RU-H3R rotating anode generator with R-Axis IV++ image plate detector) or on beamline ID29 at the ESRF (Grenoble). The data sets were subsequently processed using DENZO,[76] in space group $P2_1$ with unit cell dimensions isomorphous to those of the previously solved apo Chk1 structure.[29] The ligand bound structures were solved by molecular replacement using the apo Chk1 model coordinates (PDB code: 1AI8). Twenty cycles of rigid-body and restrained refinement were carried out followed by model building using the molecular graphics program O.[77] Crystallographic water molecules were added by cycling REFMAC5 with ARP/wARP.[78] The progress of the refinement was assessed using R_{free} and the conventional R factor. Once refinement of the structure was completed, the structures were validated using PROCHECK[79] and various programs from the CCP4i package.[80] Full data collection and refinement statistics are presented in Table 2.

4.5. Synthetic chemistry

Full experimental details for the preparation of compound **1** were described previously,[24] and only a summary of the synthetic route is outlined in Schemes 1, 2 and the following. 6-Aminoindazole was dissolved in water and treated with concentrated hydrochloric acid and sodium nitrite at 0 °C to give the corresponding diazonium salt, which was immediately converted to **4** upon treatment with potassium iodide. N-protection with mesitylenesulfonyl chloride and *tert*-sodium butoxide in THF gave sulfonamide **5**. This was then coupled to boronic acid **12** using standard Suzuki coupling conditions giving the biaryl **6**. The boronic acid **12** was prepared by treatment of protected bromide **11** with butyllithium followed by trimethyl borate (Scheme 2). Biaryl **6** was deprotected in the presence of methanolic sodium hydroxide to give the free indazole **7**, which upon iodination in the presence of sodium hydroxide and iodine gave the 3-iodoindazole **8**. Reaction of **8** with a 1:1 mixture of phenyllithium and *sec*-butyllithium followed by quenching with DMF at −78 °C gave the corresponding aldehyde **9**. The aldehyde was condensed with diaminobenzene in a mixture of methanol and water, yielding **10**. This was subsequently deprotected upon treatment with TFA in THF and water, giving compound **1**. Mass spectrometry and NMR characterisation were identical to literature:[24] MS EI *m/e* 357 (M^++H); ^{1}NMR (MeOD) δ: 3.95 (3H, s); 6.85–6.87 (1H, m); 7.15–7.20 (1H, m); 7.25–7.35 (4H, m); 7.55–7.60 (1H, m), 7.65 (1H, s); 8.45–8.50 (1H, m).

Compound **2** was prepared as follows. The commercially available acid **13** was reduced with lithium aluminium hydride giving the primary alcohol **14** in 50% yield. This was then N-protected with BOC anhydride and subsequently oxidized using the IBX system[81] in refluxing THF, yielding the 3-formyl indazole **16**. This was then reacted with *o*-phenylenediamine and molecular sulfur in DMF at 95 °C overnight giving the fully deprotected indazole-benzimidazole **2**. Mass spectrometry and NMR characterisation were identical to literature[27]: MS EI *m/e* 235 (M^++H); ^{1}NMR (MeOD) δ: 7.21–7.25 (3H, m); 7.35–7.47 (1H, m); 7.45–7.65 (3H, m), 8.35–8.40 (1H, m).

Acknowledgments

We thank the support staff of beamline ID29 at the European Synchrotron Radiation Source (Grenoble, France) for help with data collection. We thank Jenifer Borgononi, Claire Nunns, Alan Robertson, Allan Surgenor, and Lee Walmsey for assistance with the present work. We also thank I-Jen Chen and Christine Richardson for helpful discussions.

Supplementary data

Supplementary data associated with this article can be found, in the online version, at doi:10.1016/j.bmc.2005.10.022.

References and notes

1. Sanchez, Y.; Wong, C.; Thoma, R. S.; Richman, R.; Wu, Z.; Piwnica-Worms, H.; Elledge, S. J. *Science* **1977**, *277*, 1497–1501.
2. Melo, J.; Toczyski, D. *Curr. Opin. Cell Biol.* **2002**, *14*, 237–245.
3. Rhind, N.; Russell, P. *J. Cell Sci.* **2000**, *113*, 3889–3896.
4. Chen, Z.; Xiao, Z.; Chen, J.; Ng, S.-C.; Sowin, T.; Sham, H.; Rosenberg, S.; Fesik, S.; Zhang, H. *Mol. Cancer Therap.* **2003**, *2*, 543–548.
5. Liu, Q.; Guntuku, S.; Cui, X. S.; Matsuoka, S.; Cortez, D.; Tamai, K.; Luo, G.; Carattini-Rivera, S.; De Mayo, F.; Bradley, A.; Donehower, L. A.; Elledge, S. J. *Genes Dev.* **2000**, *14*, 2448–2459.

6. Zachos, G.; Rainey, M. D.; Gillespie, D. A. F. *EMBO J.* **2003**, *22*, 713–723.
7. Luo, Y.; Rockow-Magone, S. K.; Kroeger, P. E.; Frost, L.; Chen, Z.; Han, E. K.-H.; Ng, S.-C.; Simmer, R. L.; Giranda, V. L. *Neoplasia* **2001**, *3*, 411–419.
8. Lopez-Girona, A.; Tanaka, K.; Chen, X.-B.; Baber, B. A.; McGowan, C. H.; Russell, P. *Proc. Natl. Acad. Sci. U.S.A.* **2001**, *98*, 11289–11294.
9. Curman, D.; Cinel, B.; Williams, D. E.; Rundle, N.; Block, W. D.; Goodarzi, A. A.; Hutchins, J. R.; Clarke, P. R.; Zhou, B.-B.; Lees-Miller, S. P.; Andersen, R. J.; Roberge, M. *J. Biol. Chem.* **2001**, *21*, 17914–17919.
10. Furnari, B.; Rhind, N.; Russell, P. *Science* **1997**, *277*, 1495–1497.
11. Li, Q.; Zhu, G.-D. *Curr. Topics Med. Chem.* **2002**, *2*, 939–971.
12. Tenzer, A.; Pruschy, M. *Curr. Med. Chem.* **2003**, *3*, 35–46.
13. Sausville, E. A.; Arbuck, S. G.; Messmann, R.; Headlee, D.; Lush, R. D.; Bauer, K.; Murgo, A.; Figg, W. D.; Lahusen, T.; Jaken, S.; Roberge, M.; Fuse, E.; Kuwabara, T.; Senderowicz, A. M. *J. Clin. Oncol.* **2001**, *19*, 2319–2333.
14. Senderowicz, A. M. *The Oncologist* **2002**, *7*, 12–19.
15. Graves, P. R.; Yu, L.; Schwarz, J. K.; Gales, J.; Sausville, E. A.; O'Connor, P. M.; Piwnica-Worms, H. *J. Biol. Chem.* **2000**, *275*, 5600–5605.
16. Busby, E. C.; Leistritz, D. F.; Abraham, R. T.; Karnitz, L. M.; Sarkaria, J. N. *Cancer Res.* **2000**, *2000*, 2108–2112.
17. Jackson, J. R.; Gilmartin, A.; Imburgia, C.; Winkler, J. D.; Marshall, L. A.; Roshak, A. *Cancer Res.* **2000**, *60*, 566–572.
18. Zhao, B.; Bower, M. J.; McDevitt, P. J.; Zhao, H.; Davis, S. T.; Johanson, K. O.; Green, S. M.; Concha, N. O.; Zhou, B.-B. *J. Biol. Chem.* **2002**, *277*, 44609–44615.
19. Lyne, P. D.; Kenny, P. W.; Cosgrove, D. A.; Deng, C.; Zabludoff, S.; Wendoloski, J. J.; Ashwell, S. *J. Med. Chem.* **2004**, *47*, 1962–1968.
20. Kawabe, T. *Mol. Cancer Ther.* **2004**, *3*, 513–519.
21. Eastman, A.; Kohn, E. A.; Brown, M. K.; Rathman, J.; Livingstone, M.; Blank, D. H.; Gribble, G. W. *Mol. Cancer Therap.* **2002**, *1*, 1067–1078.
22. Roberge, M.; Berlinck, R. G. S.; Xu, L.; Anderson, H. J.; Lim, L. Y.; Curman, D.; Stringer, C. M.; Friend, S. H.; Davies, P.; Vincent, I.; Haggarty, S. J.; Kelly, M. T.; Britton, R.; Piers, E.; Anderson, R. J. *Cancer Res.* **1998**, *58*, 5701–5706.
23. Kohn, E. A.; Yoo, C. J.; Eastman, A. *Cancer Res.* **2003**, *63*, 31–35.
24. Kania, R. S.; Bender, S. L.; Borchardt, A.; Braganza, J. F.; Cripps, S. J.; Hua, Y.; Johnson, M. D.; Johnson, T. O. J.; Luu, H. T.; Palmer, C. L.; Reich, S. H.; Tempczyk-Russell, A. M.; Teng, M.; Thomas, C.; Varney, M. D.; Wallace, M. B. *Patent WO 0102369* **2001**.
25. Foloppe, N.; Fisher, L. M.; Howes, R.; Kierstan, P.; Potter, A.; Robertson, A. G. S.; Surgenor, A. E. *J. Med. Chem.* **2005**, *48*, 4332–4345.
26. Wang, G.; Li, G.; Mantei, R. A.; Chen, Z.; Kovar, P.; Gu, W.; Xiao, Z.; Zhang, H.; Sham, H. L.; Sowin, T.; Rosenberg, S.; Lin, N.-H. *J. Med. Chem.* **2005**, *48*, 3118–3121.
27. Edwards, M. L.; Cox, P. J.; Amendola, S.; Deprets, S. D.; Gillepsy, T. A.; Edlin, C. D.; Morley, A. D.; Gardner, C. J.; Pedgrift, B.; Bouchard, H.; Babin, D.; Gauzy, L.; Le Brun, A.; Majid, T. N.; Reader, J. C.; Payne, L. J.; Khan, N. M.; Cherry, M. *Patent WO 03/035065* **2003**.
28. Berman, H. M.; Westbrook, J.; Feng, Z.; Gilliland, G.; Bhat, T. N.; Weissig, H.; Shindyalov, I. N.; Bourne, P. E. *Nucleic Acids Res.* **2000**, *28*, 235–242.
29. Chen, P.; Luo, C.; Deng, Y.; Ryan, K.; Register, J.; Margosiak, S.; Tempczyk-Russell, A.; Nguyen, B.; Myers, P.; Lundgren, K.; Kan, C.-C.; O'Connor, P. M. *Cell* **2000**, *100*, 681–692.
30. Fersht, A. *Trends Biochem. Sci.* **1987**, *12*, 301–304.
31. Davis, A. M.; Teague, S. J. *Angew. Chem. Int. Ed.* **1999**, *38*, 736–749.
32. Hünenberger, P. H.; Helms, V.; Narayana, N.; Taylor, S. S.; McCammon, J. A. *Biochemistry* **1999**, *38*, 2358–2366.
33. Sutor, D. J. *Nature* **1962**, *195*, 68–69.
34. Taylor, R.; Kennard, O. *J. Am. Chem. Soc.* **1982**, *104*, 5063–5070.
35. Gu, Y.; Kar, T.; Scheiner, S. *J. Am. Chem. Soc.* **1999**, *121*, 9411–9422.
36. Desiraju, G. R.; T., S. *The Weak Hydrogen Bond In Structural Chemistry and Biology*; Oxford Science Publications, 1999; Vol. 9.
37. Steiner, T. *New J. Chem.* **1998**, 1099–1103.
38. Pierce, A. C.; Sandretto, K. L.; Bemis, G. W. *Proteins* **2002**, *49*, 567–576.
39. Moras, D.; Klaholz, B. P. *Structure* **2002**, *10*, 1197–1204.
40. Sarkhel, S.; Desiraju, G. R. *Proteins* **2004**, *54*, 247–259.
41. Levitt, M.; Perutz, M. F. *J. Mol. Biol.* **1988**, *201*, 751–754.
42. Meyer, E. A.; Castellano, R. K.; Diederich, F. *Angewandte Chemie* **2003**, *42*, 1210–1250.
43. Steiner, T.; Koellner, G. *J. Mol. Biol.* **2001**, *305*, 535–557.
44. Scheiner, S.; Kar, T.; Pattanayak, J. *J. Am. Chem. Soc.* **2002**, *124*, 13257–13264.
45. Brandl, M.; Weiss, M. S.; Jabs, A.; Sühnel, J.; Hilgenfeld, R. *J. Mol. Biol.* **2001**, *307*, 357–377.
46. Nakagawa, Y.; Ire, K.; Yanagita, R. C.; Hhigashi, H.; Tsuda, K. *J. Am. Chem. Soc.* **2005**, *127*, 5746–5747.
47. Nishio, M.; Umezawa, Y.; Hirota, M.; Takeuchi, Y. *Tetrahedron* **1995**, *51*, 8665–8701.
48. Dunitz, J. D. *Science* **1994**, *264*, 670.
49. Schlegel, H. B.; Gund, P.; Fluder, E. M. *J. Am. Chem. Soc.* **1982**, *104*, 5347–5351.
50. Clegg, W.; Nichol, G. S. *Acta Cryst. E* **2004**, *60*, 1433–1436.
51. Kollman, P. A. *Chem. Rev.* **1993**, *93*, 2395–2417.
52. Pearlman, D. A.; Charifson, P. S. *J. Med. Chem.* **2001**, *44*, 3417–3423.
53. Manning, G.; Whyte, D. B.; Martinez, R.; Hunter, T.; Sudarsanam, S. *Science* **2002**, *298*, 1912–1934.
54. Toledo, L. M.; Lydon, N. B.; Elbaum, D. *Curr. Med. Chem.* **1999**, *6*, 775–805.
55. Williams, D. H.; Mitchell, T. *Curr. Opin. Pharmacol.* **2002**, *2*, 567–573.
56. Noble, M. E.; Endicott, J. A.; Johnson, L. N. *Science* **2004**, *303*, 1800–1805.
57. Shao, R.-G.; Cao, C.-X.; Shimizu, T.; O'Connor, P. M.; Kohn, K. W.; Pommier, Y. *Cancer Res.* **1997**, *57*, 4029–4035.
58. Jin, P.; Gu, Y.; Morgan, D. O. *J. Cell Biol.* **1996**, *134*, 963–970.
59. Poon, R. Y. C.; Jiang, W.; Toyoshima, H.; Hunter, T. *J. Biol. Chem.* **1996**, *271*, 13283–13291.
60. Rhind, N.; Furnari, B.; Russell, P. *Genes Dev.* **1997**, *11*, 504–511.
61. Morley, S. D.; Afshar, M. *J. Comput. Aided Mol. Des.* **2004**, *18*, 189–208.
62. Barril, X.; Hubbard, R. E.; Morley, D. *Mini-Rev. Med. Chem.* **2004**, *4*, 779–791.
63. Morley, D. *in preparation*.
64. MacKerell, A. D., Jr.; Bashford, D.; Bellott, M.; Dunbrack, R. L., Jr.; Evanseck, J. D.; Field, M. J.; Fisher, S.; Gao, J.; Guo, H.; Ha, S.; Joseph-McCarthy, D.; Kuchnir, L.; Kuczera, K.; Lau, F. T. K.; Mattos, C.; Michnick, S.; Ngo, T.; Nguyen, D. T.; Prodhom, B.; Reiher, W. E., III; Roux, B.; Schlenkrich, M.; Smith, J. C.; Stote, R.; Straub,

J.; Watanabe, M.; Wiórkiewicz-Kuczera, J.; Yin, D.; Karplus, M. *J. Phys. Chem. B* **1998**, *102*, 3586–3616.
65. http://www.chemcomp.com.
66. Halgren, T. *J. Comp. Chem.* **1999**, *20*, 720–729.
67. Hardcastle, I. R.; Arris, C. E.; Bentley, J.; Boyle, F. T.; Chen, Y.; Curtin, N. J.; Endicott, J. A.; Gibson, A. E.; Golding, B. T.; Griffin, R. J.; Jewsbury, P.; Meneyrol, J.; Mesguiche, V.; Newell, D. R.; Noble, M. E. M.; Pratt, D. J.; Wang, L.-Z.; Whitfield, H. J. *J. Med. Chem.* **2004**, *47*, 3710.
68. O'Donovan, C.; Martin, M. J.; Gattiker, A.; Gasteiger, E.; Bairoch, A.; Apweiler, R. *Brief Bioinform.* **2002**, *3*, 275–284.
69. Chothia, C.; Lesk, A. M. *EMBO J.* **1986**, *5*, 823–826.
70. Martí-Renom, M. A.; Stuart, A. C.; Fiser, A.; Sánchez, R.; Melo, F.; Šali, A. *Annu. Rev. Biophys. Biomol. Struct.* **2000**, *29*, 291–325.
71. Levitt, M. *J. Mol. Biol.* **1992**, *226*, 507–533.
72. Fechteler, T.; Dengler, U.; Schomberg, D. *J. Mol. Biol.* **1995**, *253*, 114–131.
73. Delano, W. L. *The PyMOL User's Manual*; DeLano Scientific: San Carlos, CA, USA, 2002.
74. Kakkar, T.; Boxenbaum, H.; Mayersohn, M. *Drug Metab. Dispos.* **1999**, *27*, 756–762.
75. http://www.idbs.com.
76. Otwinowski, Z.; Minor, W. *Methods Enzymol.* **1997**, *276*, 307–326.
77. Jones, T. A.; Kjelgaard, M. *Uppsala University, Uppsala, Sweden* **1993**.
78. Perrakis, A.; Morris, R. J. H.; Lamzin, V. S. *Nat. Struct. Biol.* **1999**, *6*, 458–463.
79. Laskowwski, R. A.; MacArthur, M. W.; Moss, D. S.; Thornton, J. M. *J. Appl. Crystallogr.* **1993**, *26*, 283–291.
80. Collaborative Computational Project, N. *Acta Cryst. D* **1994**, *50*, 760–763.
81. Frigerio, M.; Santagostino, M.; Sputore, S. *J. Org. Chem.* **1999**, *64*, 4537–4538.
82. Yang, J.; Cron, P.; Good, V. M.; Thompson, V.; Hemmings, V.; Barford, D. *Nat. Struct. Biol.* **2002**, *9*, 940–944.
83. Bhat, R.; Xue, Y.; Berg, S.; Hellberg, S.; Ormo, M.; Nilsson, Y.; Radesater, A. C.; Jerning, E.; Markgren, P. O.; Borgegard, T.; Nylof, M.; Gimenez-Cassina, A.; Hernandez, F.; Lucas, J. J.; Diaz-Nido, J.; Avila, J. *J. Biol. Chem.* **2003**, *278*, 45937–45945.
84. Biondi, R. M.; Komander, D.; Thomas, C. C.; Lizcarno, J. M.; Deak, M.; Alessi, D. R.; van Aalten, D. M. F. *EMBO J.* **2003**, *21*, 4219–4228.
85. Zheng, J. H.; Trafny, E. A.; Knighton, D. R.; Xuong, N. H.; Taylor, S. S.; Teneyck, L. F.; Sowadsky, J. M. *Acta Cryst. D Biol. Cryst.* **1993**, *49*, 362.
86. Kakkar, T.; Pak, Y.; Mayersohn, M. *J. Pharmacol. Exp. Ther.* **2000**, *293*, 861–869.